Meteoritics & Planetary Science 38, Nr 12, 1713–1731 (2003)
Abstract available online at http://meteoritics.org

A petrogenetic model for the origin and compositional variation of the martian basaltic meteorites

Lars E. BORG* and David S. DRAPER

Institute of Meteoritics, Department of Earth and Planetary Scienes, University of New Mexico, Albuquerque, New Mexico 87131, USA
*Corresponding author. E-mail: lborg@unm.edu

(Received 22 April 2003; revision accepted 18 December 2003)

Abstract–The major element, trace element, and isotopic compositional ranges of the martian basaltic meteorite source regions have been modeled assuming that planetary differentiation resulted from crystallization of a magma ocean. The models are based on low to high pressure phase relationships estimated from experimental runs and estimates of the composition of silicate Mars from the literature. These models attempt to constrain the mechanisms by which the martian meteorites obtained their superchondritic CaO/Al_2O_3 ratios and their source regions obtained their parent/daughter ($^{87}Rb/^{86}Sr$, $^{147}Sm/^{144}Nd$, and $^{176}Lu/^{177}Hf$) ratios calculated from the initial Sr, Nd, and Hf isotopic compositions of the meteorites. High pressure experiments suggest that majoritic garnet is the liquidus phase for Mars relevant compositions at or above 12 GPa. Early crystallization of this phase from a martian magma ocean yields a liquid characterized by an elevated CaO/Al_2O_3 ratio and a high Mg#. Olivine-pyroxene-garnet-dominated cumulates that crystallize subsequently will also be characterized by superchondritic CaO/Al_2O_3 ratios. Melting of these cumulates yields liquids with major element compositions that are similar to calculated parental melts of the martian meteorites. Furthermore, crystallization models demonstrate that some of these cumulates have parent/daughter ratios that are similar to those calculated for the most incompatible-element-depleted source region (i.e., that of the meteorite Queen Alexandra [QUE] 94201).

The incompatible-element abundances of the most depleted (QUE 94201-like) source region have also been calculated and provide an estimate of the composition of depleted martian mantle. The incompatible-element pattern of depleted martian mantle calculated here is very similar to the pattern estimated for depleted Earth's mantle. Melting the depleted martian mantle composition reproduces the abundances of many incompatible elements in the parental melt of QUE 94201 (e.g., Ba, Th, K, P, Hf, Zr, and heavy rare earth elements) fairly well but does not reproduce the abundances of Rb, U, Ta and light rare earth elements. The source regions for meteorites such as Shergotty are successfully modeled as mixtures of depleted martian mantle and a late stage liquid trapped in the magma ocean cumulate pile. Melting of this hybrid source yields liquids with major element abundances and incompatible-element patterns that are very similar to the Shergotty bulk rock.

INTRODUCTION

The basaltic martian meteorites (shergottites) demonstrate a huge range of trace element and isotopic compositions, indicating that they are derived from a variety of distinct sources (McSween 1994; Borg et al. 2002). One end of the compositional continuum is defined by meteorites such as QUE 94201 (QUE) that are characterized by rare earth element (REE) patterns showing light REE (LREE) depletions and radiogenic isotopic compositions indicative of being derived from source regions with long-term depletions in incompatible elements. The other end of the continuum is represented by meteorites, like Shergotty, that have flat REE patterns and radiogenic isotopic compositions indicative of being derived from source regions with long-term enrichments in incompatible elements. Short-lived chronometers, such as $^{146}Sm \rightarrow {}^{142}Nd$ ($t_{½}$ = 103 Ma) indicate that the source regions of the martian basalts formed at ~4.52 ± 0.02 Ga (Harper et al. 1995; Borg et al. 1997a, 2003).

These observations have led to 2 scenarios for the generation of the compositional variations observed in the meteorite suite. In the first, compositional variation is attributed to differentiation of mantle-derived magmas by assimilation of martian crust accompanied by fractional

crystallization (AFC; Jones 1989; Borg et al. 1997b; Herd et al. 2002). One of the main inconsistencies with this scenario is that martian basaltic meteorites demonstrate little correlation between mineralogical or geochemical indices of differentiation (for example, SiO_2 or Mg#, molar Mg/Mg + Fe) and incompatible-trace-element abundances, ratios, or isotopic compositions (Fig. 1). This is perhaps most clearly manifest by meteorites, such as NWA 1068, that are derived from silica-poor parental magmas with very mafic major-element compositions but are also strongly enriched in incompatible elements (Barrat et al. 2002; Mikouchi and Miyamoto 2002; Shih et al. 2003). In the second scenario, compositional variations result from melting of ancient and compositionally distinct mantle source regions. The formation of such source regions early in the history of Mars is consistent with the presence of a magma ocean (Borg et al. 1997a, 2003; Blichert-Toft et al. 1999; Brandon et al. 2000; Hess 2002). Thus, the extreme compositional and isotopic variations observed in the martian basaltic meteorite suite is attributed to mixing variable proportions of melts derived from mafic cumulates and late stage crystallization products i.e., trapped liquids (Borg et al. 1997a, 2003). In fact, Borg et al. (2003) have calculated the parent/daughter ratios (i.e., $^{87}Rb/^{86}Sr$, $^{147}Sm/^{144}Nd$, and $^{176}Lu/^{177}Hf$ ratios) of the shergottite sources from their Rb-Sr, Sm-Nd, and Lu-Hf isotopic systematics assuming source formation at ~4.51 Ga (Table 1). This study suggests that the source regions of the shergottites are mixtures of mafic cumulates and a late stage trapped liquid (that is, the last crystallized remnant of the original magma ocean) characterized by strong incompatible-element enrichments (Fig. 2). This scenario is appealing because it also accounts for the lack of evidence for differentiation by AFC and the fact that all of the martian parental melts are broadly basaltic despite large variations in their trace element and isotopic compositions.

Constraining the composition of the martian meteorite source regions is a complicated task. Despite minimal evidence for differentiation by AFC, many of the meteorites are highly differentiated. Differentiation is reflected by the fact that most martian basalt parental liquids are estimated to have Mg#s that are less than 65 (Stolper and McSween 1979; McSween and Jarosewich 1983; Treiman 1986; Longhi and Pan 1988; McSween et al. 1988; Harvey et al. 1993; McSween et al. 1996) and, therefore, are unlikely to represent primary melts in equilibrium with their sources at the time of melt extraction. In addition, many of the meteorites have accumulated significant amounts of minerals (Stolper and McSween 1979; McSween 1985, 1994). Therefore, reconstructing the mineralogy, major element, or trace element compositions of the source regions using a backward modeling approach (i.e., determine the composition of the source from the composition of the meteorites) is very difficult. The goal of the modeling presented below is to estimate trace element ratios and

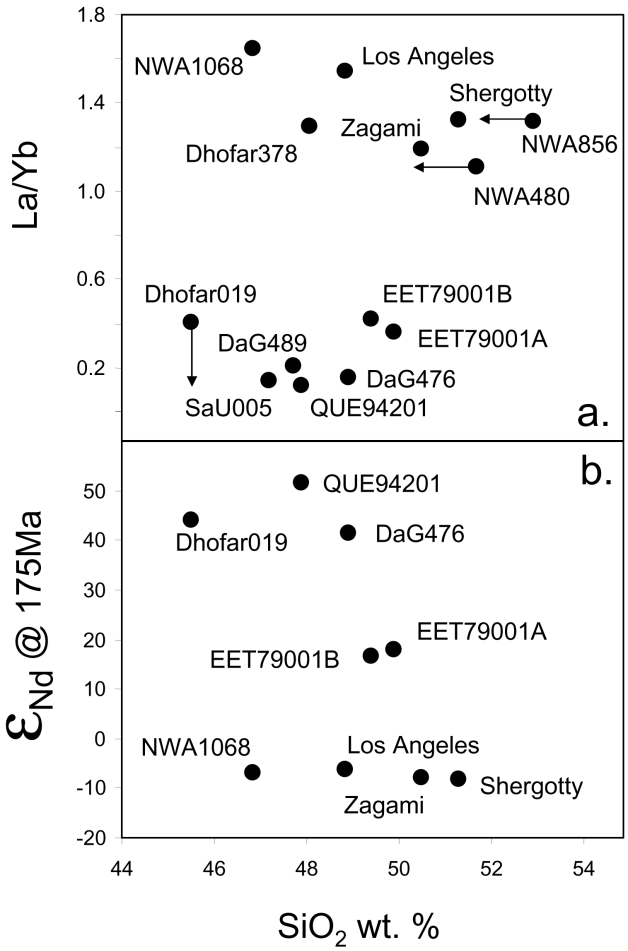

Fig. 1. Bulk rock SiO_2 versus La/Yb ratios and ε_{Nd} calculated at 175 Ma for basaltic martian meteorites. The lack of correlation on both of these diagrams is inconsistent with compositional variation resulting from assimilation-fractional crystallization. The left arrows on (a) indicate that SiO_2 was calculated by difference as per McSween et al. (2003) and, therefore, represents maximum values. The down arrow on this figure indicates that the La/Yb ratio of Dhofar 019 could have been increased by terrestrial alteration (Taylor et al. 2002). The Nd isotopic data are derived from Sm-Nd isochrons and are unlikely to be affected by terrestrial alteration. The isotopic data summarized in Borg et al. (2003) and most of the elemental data represent averages of Lodders and Fegley (1998). Additional elemental data for Si, La, and Yb are from single samples in which all 3 elements were analyzed (Meyer 2003).

abundances of the martian meteorite source regions, assuming that they formed as a result of crystallization of a martian magma ocean. This forward approach to the geochemical modeling of the compositions of the shergottite source regions is adopted because it is independent of the major and trace element compositions of the meteorites themselves. The models are constrained by experimental results at low and high pressure and the results of radiogenic isotope studies. The modeling indicates that much of the major and trace element systematics observed in the meteorite suite are consistent with the melting of mafic

Table 1. Parent/daughter ratios of martian basaltic meteorite sources.[a]

	Age (Ma)	$^{87}Rb/^{86}Sr$	$^{147}S/^{144}Nd$	$^{176}Lu/^{177}Hf$
Shergotty	165	0.374	0.182	0.0279
Zagami	177	0.357	0.187	0.0276
LA1	170	0.349	0.186	–
EET 79001A	173	0.209	0.224	0.0444
EET 79001B	173	0.215	0.226	0.0441
ALH 77005	179	0.183	0.217	0.0439
LEW 88516	178	0.178	0.212	–
DaG 476	474	0.037	0.267	–
QUE 94201	327	0.037	0.285	0.0482

[a]Parent/daughter ratios of meteorite source regions are calculated from initial Sr, Nd, Hf isotopic compositions assuming differentiation at 4.513 Ga. The data are from Borg et al. (2003). The initial Sr and Nd isotopic compositions are determined from mineral isochrons except for EET B (Nd) and DaG (Sr). The initial Hf isotopic compositions are calculated from whole rock isotopic compositions using preferred ages of Nyquist et al. (2001). The calculations assume that undifferentiated source regions had chondritic Sm-Nd and Lu-Hf isotopic systematics and Rb-Sr isotopic systematics estimated for bulk Mars (see text). The decay constants used in modeling are: $\lambda(^{87}Rb) = 0.01402\ (Ga)^{-1}$; $\lambda(^{147}Sm) = 0.00654\ (Ga)^{-1}$; $\lambda(^{176}Lu) = 0.0193\ (Ga)^{-1}$. The data are from (Blichert-Toft et al. 1999); Borg et al. (1997a, 2002, 2003), (Nyquist et al. 1979, 1995, 2000, 2001); and Wooden et al. (1982).

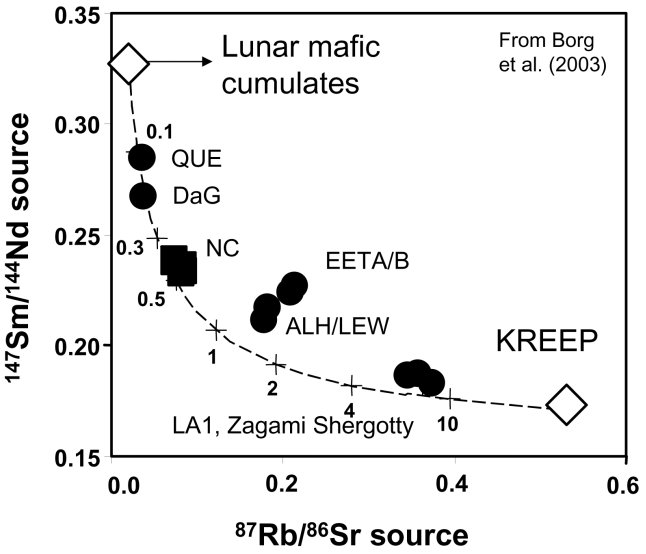

Fig. 2. Plot of parent/daughter ratios ($^{87}Rb/^{86}Sr$ and $^{147}Sm/^{144}Nd$) calculated for martian meteorite sources. Parent/daughter ratios are calculated from initial Sr and Nd isotopic compositions of the shergottites (filled circles) and nakhlites (filled squares), assuming differentiation from bulk Mars at 4.513 Ga. The open diamonds represent lunar sources used as end members for mixing curve (dashed line). Note that the sources of the martian meteorites lie on the mixing array between a mafic lunar source and a component enriched in K, REE, and P (KREEP) that are most likely produced as a result of crystallization of a magma ocean. The figure and data references are in Borg et al. (2003).

cumulates and late-stage crystallization products of a martian magma ocean.

APPROACH TO MODELING

The approach to modeling adopted below is similar to that outlined by Snyder et al. (1992) for the Moon. The first step is to estimate a crystallization sequence for the martian magma ocean. The crystallization sequence is based on the results of low to high pressure experimental runs on appropriate bulk compositions. The applicability of the crystallization sequence is tested using modal partial melting models that permit the calculated melt compositions of the various cumulate packages to be directly compared to the estimated compositions of martian basalt parental liquids. The most mafic parental melt composition is that calculated for lherzolitic shergottite ALH 77005 (ALH) by McSween et al. (1988), termed Am. This composition is used for comparison because it demonstrates the least evidence of differentiation.

Next, the trace element compositions of individual cumulate packages are calculated using their estimated mineral modes and a combination of equilibrium and fractional crystallization models. The $^{87}Rb/^{86}Sr$, $^{147}Sm/^{144}Nd$, and $^{176}Lu/^{177}Hf$ ratios of the modeled cumulates are compared to the ratios calculated for the most depleted source region from the initial isotopic compositions of QUE by Borg et al. (2003). The mineralogy and composition of the cumulate that best reproduces the parent/daughter ratios calculated for the QUE source region is used to define depleted martian mantle (DMM). The composition of partial melts of DMM are then calculated to determine if the trace element composition of QUE is consistent with being derived from DMM. More evolved meteorites, such as Shergotty, are modeled as melts of a mixture of DMM and late stage liquids trapped in the cumulate pile during crystallization of the martian magma ocean.

It is important to emphasize that the model results represent the best constraints that can be placed on the mineralogy and compositions of the martian meteorite source regions based on the existing experimental and isotopic data, assuming planetary differentiation resulted from the crystallization of a magma ocean. This exercise is, therefore, intended to elucidate which geochemical and isotopic parameters present in the shergottite meteorite suite are consistent with a magma ocean hypothesis of differentiation and which characteristics are not.

MAJOR ELEMENT CRYSTALLIZATION AND MELTING MODELS

In this section, a 2-stage model for martian basaltic magmatism is described. The model is intended to approximate initial martian magma ocean solidification and subsequent melting of magma ocean cumulates to produce liquids that are parental to the martian meteorites. The goal of the modeling is to determine whether magma ocean differentiation processes can produce: 1) martian magma source regions with the appropriate trace element and isotopic characteristics; and 2) parental liquids with the appropriate major and trace element compositions. The models are in the general style of those constructed by Snyder et al. (1992) but have some significant differences. The first stage of the model is the crystallization stage, and the second is the melting stage. In the crystallization stage, crystallization of a martian magma ocean results in the generation of a series of cumulate packages. These packages are defined by a change in the mineral mode of the crystallizing assemblage. In the melting stage, these cumulates are melted to produce the potential martian meteorite parental liquids.

In order to model the crystallization stage, we must infer a reasonable crystallization sequence by which a martian magma ocean is expected to solidify. Snyder et al. (1992) used low pressure phase equilibria and computer models adjusted for a lunar bulk composition to predict a crystallization sequence of the lunar magma ocean. Unfortunately, such numerical models are not yet mature enough at the higher pressure range that is potentially pertinent to the crystallization of a magma ocean on a relatively large planet such as Mars. Furthermore, as described below, experimental coverage for Mars-relevant compositions is not as complete as for the Moon. As a result of these limitations, the crystallization sequences for the martian magma ocean, although based on phase relations determined experimentally at low to high pressures, are not rigorously defined. The intent is not to presume that these are the only crystallization sequences possible during early differentiation of the martian magma ocean. Rather, we are simply making reasonable choices that are based on petrologic common sense and what few data on high pressure phase relations are available for materials of appropriate compositions.

The Mineral Modes of Martian Magma Ocean Cumulates

Experimental Constraints on Crystallization Sequences

Crystallization of a martian magma ocean presumably took place over a range of pressures, reaching approximately 15 GPa or, perhaps, greater (Ohtani et al. 1995; Blichert-Toft et al. 1999). Experimental studies at pressures this high have been performed on carbonaceous chondrite (Agee et al. 1995) and on terrestrial peridotite compositions (e.g., Ohtani et al. 1989; Zhang and Herzberg 1994; Herzberg and Zhang 1996). However, experimental data for Mars-relevant compositions (Table 2) are more limited. Near-liquidus experiments on the bulk Mars composition proposed by Dreibus and Wänke (1985; hereafter, DW), have been performed only at pressures of 2.0 GPa or less (Bertka and Holloway 1994a, b; Gilpin et al. 2001). Higher pressure work has also been completed but, thus far, has constrained only subsolidus assemblages (Bertka and Fei 1997). More recently, the L5 ordinary chondrite Homestead, similar in composition to DW, has been used as an analogue for martian mantle in near-liquidus phase equilibrium and partitioning studies at pressures up to ~10 GPa (Draper et al. 2001; Wasserman et al. 2001; Draper et al. 2003; Agee and Draper Forthcoming). A combination of experimental results from these studies is used to constrain hypothetical martian magma ocean crystallization sequences.

The experiments on Homestead L5 (Draper et al. 2001; Wasserman et al. 2001; Draper et al. 2003; Agee and Draper Forthcoming) demonstrate that, at pressures up to ~10 GPa, olivine and orthopyroxene are the liquidus phases, and garnet is a near-liquidus phase starting at ~5 GPa, apparently crystallizing closer to the liquidus with increasing pressure. Majorite is the high pressure form of garnet and consists of a solid solution between enstatite and pyrope. With increasing pressure, the solubility of the enstatite component in pyrope increases systematically such that, with increasing pressure and majorite content, garnet becomes progressively more silica-rich and alumina-poor. In addition, the crystal structure undergoes a transformation from isometric to hexoctahedral. The garnets grown at 5 GPa by Draper et al. (2003) display a small but distinct majorite content and are, hence, termed "mildly" majoritic; this majorite content increases to 9 GPa (the highest pressure studied so far by those authors), by which time majorite contents are comparable to those grown from more magnesian compositions appropriate for the terrestrial mantle. Partitioning of both major and trace elements is affected by these pressure-induced transformations. In general, the partitioning of major

Table 2. Bulk composition of Mars mantle analogues.[a]

	Homestead	DW Mars mantle	Bulk Mars
SiO_2	47.0	44.4	45.4
TiO_2	0.15	0.14	0.14
Al_2O_3	2.68	3.02	2.89
FeO	16.0	17.9	17.2
MnO	0.41	0.46	0.37
MgO	29.4	30.2	29.6
CaO	2.10	2.45	2.35
Na_2O	0.12	0.50	0.97
K_2O	0.15	0.01	0.11
P_2O_5	0.32	0.16	0.17
Total	99.32	98.78	99.20

[a]The Homestead L5 chondrite compositions are from Jarosewich and Dodd (1981, 1985). The DW is bulk Mars composition from Dreibus and Wänke (1985). The bulk silicate Mars data are from Lodders and Fegley (1997).

elements (with the exception of Si and Al) is less strongly affected by increasing majorite content than is the case for many trace elements, for example, the heavy REE. A full description of the effects on element partitioning was presented by Draper et al. (2003).

Figure 3 illustrates a convergence of mineral-in curves with increasing pressure and an apparent "kink" in the liquidus surface near 10 GPa. This suggests that garnet should become the liquidus phase at pressures above ~12 GPa by analogy with the phase relations for Allende (Agee et al. 1995) and KLB-1 (Zhang and Herzberg 1994; Herzberg and Zhang 1996). Unfortunately, experiments on the Homestead composition above 10 GPa have not yet been carried out. Nevertheless, it seems reasonable that crystallization sequences at comparatively low pressures (below 5 GPa) would be characterized by liquidus olivine, possibly plus orthopyroxene, while those at higher pressures (~15 GPa) would be characterized by liquidus or near-liquidus majoritic garnet, followed by olivine and orthopyroxene. Garnet appearing in lower pressure sequences would be largely pyropic, whereas at higher pressures, garnet would be expected to incorporate a significant majorite component (Draper et al. 2003). At both low and high pressure, late stages of crystallization are likely to involve clinopyroxene and a Ti-oxide phase such as ilmenite, although these late-stage conditions have not been explored experimentally.

Crystallization Sequences Used in Forward Modeling

Several plausible crystallization sequences are proposed for crystallization of the martian magma ocean at various pressures. These sequences are summarized in Table 3 and Fig. 4, where they are compared against the low pressure sequences proposed by Snyder et al. (1992) for the Moon. To represent conditions at approximately 3–5 GPa, a sequence similar to that used by Snyder et al. (1992) for lunar compositions was chosen, replacing plagioclase with clinopyroxene and pyropic garnet. The crystallization sequence is as follows: olivine, olivine + orthopyroxene, orthopyroxene + clinopyroxene, clinopyroxene + garnet + ilmenite, and finally, clinopyroxene + garnet. This sequence is similar to that used by Borg et al. (1997a) for modeling the Rb-Sr and Sm-Nd isotopic systematics of Mars and yields a bulk magma ocean cumulate mineral mode that is similar to that proposed for bulk Mars by Longhi et al. (1992). From approximately 5 to 10 GPa, mildly majoritic garnet is a subliquidus phase after the initial crystallization of olivine and orthopyroxene. Thus, the 10 GPa crystallization sequence used in the models is: olivine + orthopyroxene, olivine + orthopyroxene + garnet, orthopyroxene + clinopyroxene + garnet, and clinopyroxene + garnet + ilmenite. At the even higher pressure of approximately 15 GPa, an even more strongly majoritic garnet is taken to be the liquidus phase. Thus, the 15 GPa crystallization sequence used in the models is: majoritic garnet, olivine + garnet, olivine + orthopyroxene, orthopyroxene + clinopyroxene, and clinopyroxene + ilmenite.

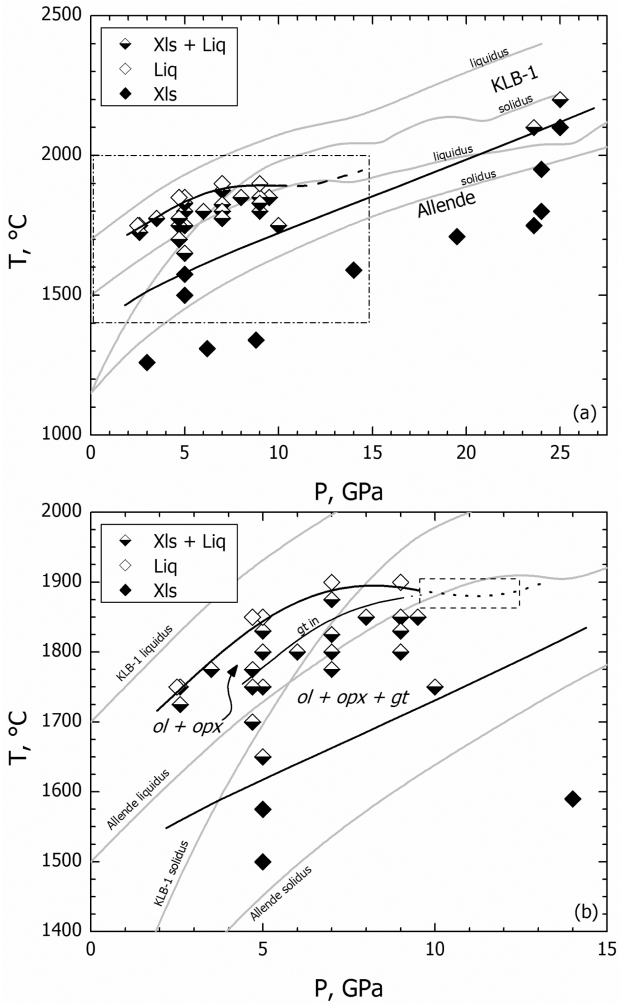

Fig. 3. Pressure-temperature summary diagrams showing phase relations of Homestead L5 (Wasserman et al. 2001; Draper et al. 2003; Agee and Draper Forthcoming) with runs above 14 GPa and subsolidus data from Shannon (unpublished thesis). The open symbols ("Liq") denote runs consisting of all liquid; the half-filled symbols ("Xls + liq") denote runs containing both crystals and liquid; the solid symbols ("Xls") denote runs with no liquid. The solidus and liquidus curves for terrestrial peridotite KLB-1 (Zhang and Herzberg 1994; Herzberg and Zhang 1996) and for Allende (Agee et al. 1995) are shown in light grey for comparison. The dashed box in (a) denotes the region shown in more detail in (b), which illustrates fields where olivine (ol), orthopyroxene (opx), and garnet (gt) coexist with melt. The "Gt in" curve in (b) shows the approximate stability of majoritic garnet in this composition. The dashed portion of the liquidus curve is estimated from lower pressure data that appear to require a "kink" in the liquidus, which is analogous to that shown for KLB-1 and Allende when garnet becomes the liquidus phase; this is consistent with the trend of the garnet-in curve. The dashed box in (b) shows the approximate P-T region where garnet is predicted to become the liquidus phase for Homestead L5.

To calculate the liquid line of descent for the martian magma ocean, the major element magma ocean crystallization models use: 1) the silicate fraction of the Homestead meteorite to represent the bulk composition of a martian magma ocean; 2) the percent crystallized solid (PCS)

Table 3 Estimated crystallization low, medium, and high pressure sequences.[a]

Sequence	PCS	Olivine	Orthopyroxene	Clinopyroxene	Garnet/Majorite	Ilmenite
Low P (~3–5 GPa)	0–40	100	–	–	–	–
	40–78	75	25	–	–	–
	78–86	–	25	75	–	–
	86–95	–	–	90	5	5
	95–98	–	–	95	5	–
	Total	69.9	11.7	17.3	0.6	0.5
Medium P (~10 GPa)	0–30	50	50	–	–	–
	30–50	40	45	–	15	–
	50–80	–	20	70	10	–
	80–98	–	–	90	5	5
	Total	23.5	30.6	38.0	7.0	0.9
High P (~15 GPa)	0–5	–	–	–	100	–
	5–20	80	–	–	20	–
	20–60	50	50	–	–	–
	60–90	–	60	40	–	–
	90–98	–	–	95	–	5
	Total	32.7	38.8	20	8.2	0.4

[a]PCS = Percent crystallization. The totals are recalculated to 100%.

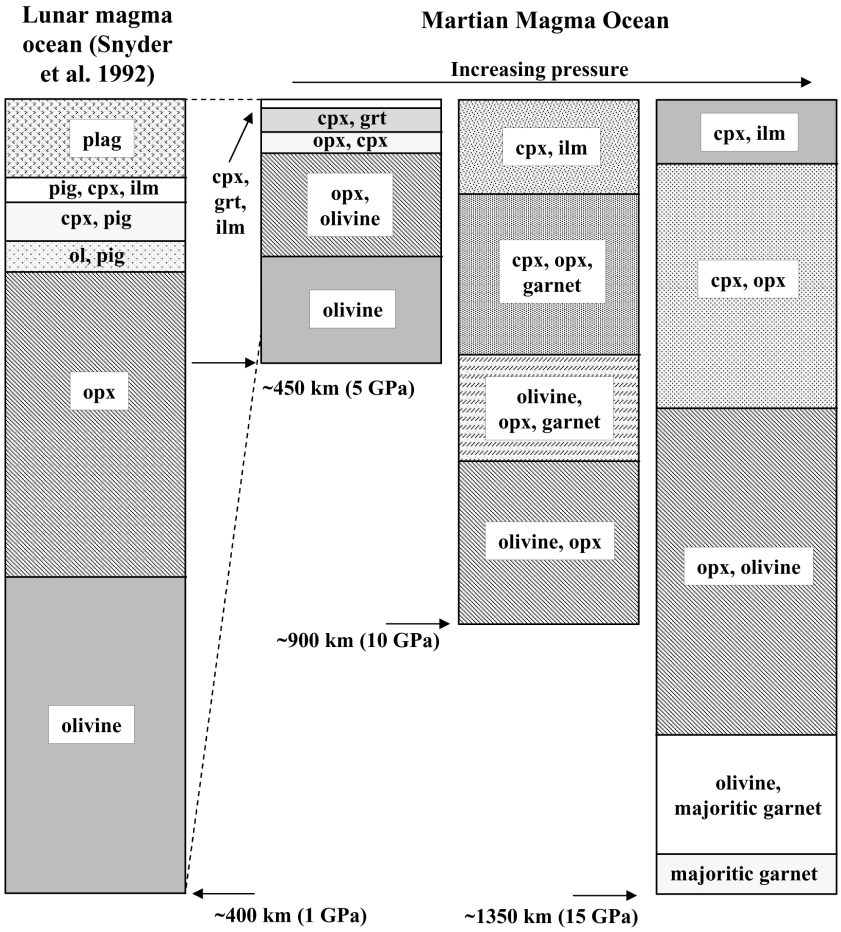

Fig. 4. Cartoon depicting crystallization sequences for a lunar and martian magma ocean. The lunar model is from Snyder et al. (1992). The low pressure (5 GPa), medium pressure (10 GPa), and high pressure (15 GPa) sequences are based on phase relationships discussed in the text. The 3 martian sequences differ primarily by when garnet becomes the liquidus phase. Note that these cartoons are not intended to mimic the stratigraphy of the martian mantle and crust but simply to represent the crystallization order and modes of a magma ocean cumulates.

steps listed in Table 3; and 3) the bulk compositions of the cumulate packages. Following Snyder et al. (1992), the compositions of liquids and cumulate packages were calculated assuming equilibrium crystallization when the fraction of melt remaining (F) was above 20 percent and assuming fractional crystallization when F was 20 percent and below. Snyder et al. (1992) used equilibrium crystallization equations to model the early stages of magma ocean crystallization because it is likely that the magma ocean would be vigorously convecting at this time, allowing minerals to be suspended and in equilibrium with the liquid. As more of the magma ocean solidifies, convection is expected to decrease, permitting fractional crystallization to become the dominant crystallization process.

The compositions of starting liquids at the beginning of each PCS step were taken to be the compositions of the liquids remaining at end of the previous step. The composition of the liquid remaining after each PCS step was calculated using partition coefficients listed in Table 4. The composition of a late stage liquid trapped in the cumulate pile after 98% crystallization is also calculated. This is the highest percent crystallization for which our major element models are likely to be even partially reliable. The major element partition coefficients are from Draper et al. (2003) for olivine, orthopyroxene, and mildly majoritic garnet and from Ohtani et al. (1989) for more strongly majoritic garnet appropriate for the 15 GPa models. The major element partition coefficients for clinopyroxene and ilmenite are from Draper and Johnston (1992) and Green and Pearson (1987), respectively. The bulk compositions of crystalline assemblages were calculated by mass balance from the progressive melts during each PCS step.

The Major Element Compositions of Cumulate Partial Melts

The melting stage of the model uses the modal mineralogy of the individual PCS steps and the average major element compositions calculated for that cumulate package. Ten percent partial melts of the cumulate packages from each PCS step were calculated assuming modal batch melting using the partition coefficients listed in Table 4. Relatively simple melt models were adopted because the current constraints placed on petrologic processes in the martian mantle are not sufficient to justify the use of more complicated melting models. Major element compositions were calculated for partial melts of cumulates that formed in the lower (5 GPa), medium (10 GPa), and higher (15 GPa) pressure crystallization sequences. Thus, a set of 4 or 5 melt compositions from each of the 3 crystallization sequences has been produced. The calculated partial melts correspond to paths through composition space taken by these liquids, assuming progressive melting from the earliest formed package in a given sequence to the last formed packages (Fig. 5). These melt paths can be thought of as representing an integrated track of the potential compositions of partial melts of a martian magma ocean that crystallized at a particular pressure. Again, we acknowledge that these paths are not unique and that different results can be obtained by altering the parameters listed in Tables 3–4. However, as discussed below, these melt paths place limits on the ranges of potential cumulate phases that are likely to be present in the martian mantle.

Major Element Melt Model Results

Figure 5 (a–d) plots the modeled melt paths in terms of the 5 most abundant major element oxides. Compositions of parent liquids calculated for several martian meteorites are also plotted for comparison. Note that the parental melt composition for ALH (the Am composition of McSween et al. [1988]) is the most primitive (highest Mg#) of the parental melts and that the other parental melts form fields on Figs. 5a–5d that are roughly parallel to the vectors for fractionation of olivine (~Fo_{80}). This suggests that the parental melts calculated for these meteorites are likely to be affected by olivine fractionation. The Am composition is, therefore, likely to be representative of melts derived from the martian mantle most directly, although it also likely underwent some

Table 4. Major element partition coefficients used in models.

	Olivine1	Orthopyroxene[a]	Clinopyroxene[b]	Majorite[c]	Majoritic garnet[d]	Ilmenite[e]
SiO_2	0.88	1.40	0.99	1.07	1.09	0
TiO_2	0.01	0.02	0.43	0.63	0.30	50
Al_2O_3	0.10	0.55	0.67	3.06	6.50	0
FeO	0.66	0.36	0.67	0.42	0.43	4
MgO	1.81	1.36	1.82	0.88	1.12	0
CaO	0.04	0.29	1.45	0.47	0.49	0
Na_2O	0.01	0.35	0.35	0.05	0.12	0
K_2O	0.01	0.01	0.01	0.04	0.01	0
P_2O_5	0.07	0.01	0.01	0.35	0.30	0

[a]Draper et al. (2003); the D values changed little between 5 and 9 GPA.
[b]Draper and Johnson (1992).
[c]Ohtani et al. (1989); 16 GPa values.
[d]Draper et al. (2003); average D values for 5 and 9 GPa.
[e]Green and Pearson (1987).

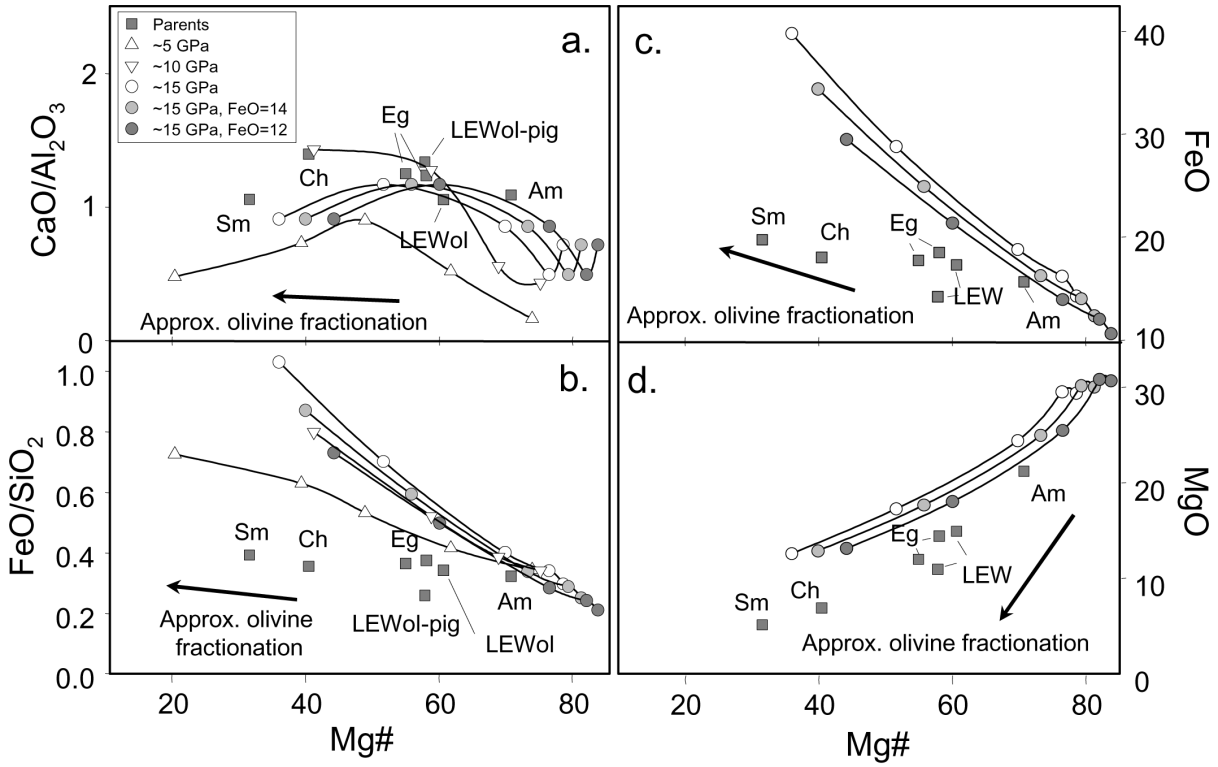

Fig. 5. Summary of major element compositions of modeled partial melts and comparison with calculated parent liquids for shergottites. Parent liquid compositions: Am, calculated by McSween et al. (1988) for ALH 77005; Eg, calculated by Longhi and Pan (1989) and Schwandt et al. (2001) for EET A79001A; LEWol and LEWol-pig, calculated by Harvey et al. (1993) assuming olivine and olivine + pigeonite saturation, respectively, for LEW 88516; Ch, calculated by Johnson et al. (1991) for Chassigny; Sm, calculated by Stolper and McSween (1979) for Shergotty. The heavy arrows show the calculated vectors for fractionation of Fo_{80} olivine. The curves denote approximate pressures of model calculations. FeO = 14 and FeO = 12 denote models calculated from an initial martian mantle having 14 and 12 wt% FeO, respectively. See text for discussion.

olivine fractionation. Nevertheless, it is the composition the major element models strive to reproduce.

From Fig. 5a, one can see that the low-pressure melts do not approach Am or any of the other parent compositions. This is largely due to their low CaO/Al_2O_3 ratios at high Mg#s, resulting from the absence of majoritic garnet as a near-liquidus phase in this sequence. The highest CaO/Al_2O_3 ratio calculated for a melt derived from the low pressure cumulate sequence has a Mg# that is significantly below Am, indicating that variations in the proportions of phases crystallizing in the modeled low pressure magma ocean will not reproduce the martian basalt parental melts. Partial melts at higher pressure show a prominent increase in CaO/Al_2O_3 ratios at high Mg#s. This suggests that garnet must be an early crystallizing phase in the martian magma ocean for partial melts of the cumulates to have the superchondritic CaO/Al_2O_3 ratios characteristic of martian basaltic magmas. However, partial melts derived from cumulates at ~10 GPa do not provide a satisfactory match to Am either. This is because garnet crystallizing at this pressure does not crystallize early enough in the sequence (Table 3) nor have a high enough majorite component (Draper et al. 2003). Cumulates forming at higher pressure near 15 GPa contain more strongly majoritic garnet and consequently yield partial melts that are closer to the composition of Am. This supports the inference that majoritic garnet must be an early phase in crystallization of a martian magma ocean.

Although the melts derived at ~15 GPa come close to reproducing the major element composition of Am, they do not match the Am composition exactly (Figs. 5c and 5d). In an effort to isolate the parameters that exert the most influence on this mismatch, other mantle bulk compositions (other chondrite types, terrestrial peridotite, etc.) were used as starting compositions in the crystallization models. Iron content was found to be the parameter to which these paths were most sensitive. Using other chondrite types, such as C and LL, resulted in no better match because these compositions have similar or even higher Fe abundances. The Homestead starting composition was therefore recalculated after arbitrarily removing 2 and 4 wt% FeO from its initial content of ~16 wt% (Table 2). Given that the composition and size of the martian core is uncertain, lower Fe in the silicate portion of Mars could reflect the presence of additional Fe in the core. Melting paths calculated using these modified starting compositions are presented on Figs. 5a–5d and are denoted "FeO = 14" and "FeO = 12," respectively. These

paths retain the shape of the 15 GPa paths, with an increase in the CaO/Al_2O_3 ratio to superchondritic levels at high Mg#. The FeO = 12 path, in particular, comes quite close to Am on Figs. 5a–5d. The comparative success of the lower Fe paths at approaching the Am composition leads to the conclusion that the martian mantle may not be as Fe-rich as has been conventionally supposed. Instead, the martian mantle could have an initial composition that is similar to that of H chondrites, with ~13.5 wt% FeO and an Mg# of ~80.

The results of our modeling suggest that the process of magma ocean crystallization followed by cumulate melting can generate partial melts that are compositionally similar to Am, the most primitive martian basalt parent melt calculated to date. This is especially true if the martian mantle is several weight percent poorer in FeO than has been thought previously. It also appears, at least in terms of compositional relations among the most abundant major elements, that the other calculated martian basalt parents can be derived from Am by simple fractionation of olivine ± orthopyroxene. It is therefore concluded that the major element compositions of the martian basalt parental liquids are consistent with the models presented here. The robustness of these major element models is tested below by determining if the trace element and isotopic systematics of the shergottites are reproduced as well.

Alternative Mechanisms to Produce Superchondritic CaO/Al_2O_3 Ratios

The basis for choosing the high pressure crystallization sequence for the martian magma ocean is the observation that the martian meteorites, and presumably the martian meteorite source regions, are characterized by low Al abundances and superchondritic CaO/Al_2O_3 ratios. An alternative view to account for these superchondritic ratios is that the "missing" aluminum may have been sequestered in martian crustal rocks via episodes of melt extraction from the martian mantle (e.g., Longhi et al. 1992). There are, in fact, indications from the Mars Pathfinder and Mars Global Surveyor missions that the martian crust may be more plagioclase-rich and, hence, more aluminous than are the basaltic meteorites. However, the precision of these measurements is not sufficient at present to obtain reliable estimates of the composition of the martian crust, although much progress has been made in recent years (McSween et al. 2003). Presumably the Mars Exploration Rover missions, en route to Mars as of late 2003, hold out promise for increasing our knowledge about the composition of the martian crust.

Even if the martian crust is, in fact, highly aluminous, separation of plagioclase-rich melts from martian mantle source regions would produce only a slight perturbation in the CaO/Al_2O_3 ratio of those sources. This is because, among the rock-forming minerals most important in mantle melting (olivines, pyroxenes, feldspars, garnets), only garnet appears capable of substantially fractionating CaO from Al_2O_3. Finally, isotopic constraints from short-lived systems mandate that any crustal extraction processes would have to be complete by no later than ~50 Ma after planetary accretion, and the reservoirs thus produced would be required to remain geochemically isolated thereafter. We believe these complications, in addition to constraints cited in previous sections, make the conceptually simpler magma-ocean model we explore here to be more appealing.

TRACE ELEMENT CRYSTALLIZATION AND MELTING MODELS

Trace element modeling was performed independently of the major element modeling and, therefore, provides a test of consistency between the 2 sets of models. The trace element compositions of the cumulate packages were calculated from the bulk Mars starting composition of Lodders and Fegley (1997) and are presented in Fig. 6a. This composition was chosen because it was the most complete and, therefore, offered the most consistent data set for trace element modeling; and its major element composition is very similar to the composition of the Homestead meteorite used to model the major element composition of the martian magma ocean (Table 2). Although the bulk Mars composition of Lodders and Fegley (1997) is slightly more Fe-rich than is the Homestead composition (Table 2), the bulk Mars composition incorporates a martian core component, whereas the Homestead composition does not. Thus, the major-element composition of bulk Mars is similar to and consistent with the major element composition used in the models.

The Rb-K, Sm, and Lu abundances of bulk Mars were adjusted by −57%, +15%, and +19%, respectively, to ensure that the bulk composition had $^{87}Rb/^{86}Sr = 0.32$ (the estimated bulk Mars value discussed by Borg et al. [2001]) and $^{147}Sm/^{144}Nd$ and $^{176}Lu/^{177}Hf$ ratios of chondritic uniform reservoir (CHUR). The high pressure magma ocean crystallization sequence (Table 3) was chosen to define the modal mineralogy of the cumulates because this sequence best reproduced the major element features (e.g., CaO/Al_2O_3 ratios) of the most mafic martian basalt parental melt (Am). The trace element composition of the evolving magma ocean liquid calculated for each cumulate package using equilibrium (F <20) or fractional (F >20) crystallization models, the modal mineralogy estimated for each PCS step, and the partition coefficients are presented in Table 5. Note that the calculated compositions are not strongly influenced by whether equilibrium or fractional crystallization models are used because almost all of the elements modeled are highly incompatible in the mineral assemblages being modeled. The partition coefficients used in the model are those summarized by Snyder et al. (1992) for a low pressure crystallization lunar magma ocean. However, the partition coefficients for garnet/majorite are from the 9 GPa data of Draper et al. (2003). The trace element compositions of the cumulates in each PCS step represent the average cumulate composition crystallizing

Table 5. Trace element partition coefficients used in melting models.[a]

Element	Olivine	Ortho-pyroxene	Clino-pyroxene	Majoritic garnet	Ilmenite	Titanite	Phlogopite	Amphibole
Rb	0.00018	0.0006	0.011	0.001	1E-05	1E-05	3.06	0.31
Ba	0.00018	0.0006	0.0165	0.0015	1E-05	1E-05	1.09	0.436
Th	0.0001	0.001	0.01	0.0001	1E-05	1E-05	0.31	0.11
U	0.0001	0.001	0.02	0.0001	1E-05	1E-05	0.21	0.15
Ta	0.01	0.025	0.05	0.08	1E-05	19	1E-05	0.38
K	7.7E-05	0.00026	0.011	0.018	1E-05	1E-05	2.7	0.4
La	0.0004	0.002	0.054	0.01	1E-05	2.1	0.036	0.17
Ce	0.0005	0.003	0.0646	0.021	1E-05	4.72	0.034	0.26
P	0.055	0.03	0.03	0.261	1E-05	1E-05	1E-05	1E-05
Sr	0.00019	0.007	0.12	0.0011	1E-05	1E-05	0.081	0.12
Nd	0.001	0.0068	0.107	0.036	1E-05	9.96	0.032	0.44
Sm	0.0013	0.01	0.17	0.103	1E-05	11	0.031	0.76
Zr	0.01	0.01	0.233	0.268	0.44	0.01	2.1	0.7
Hf	0.01	0.01	0.233	0.322	0.44	0.01	2.1	0.7
Eu	0.0016	0.013	0.28	0.22	0.001	11	0.03	0.88
Gd	0.0015	0.016	0.32	0.43	0.001	11	0.03	0.86
Tb	0.0015	0.019	0.31	0.335	0.001	11	0.032	0.78
Dy	0.0017	0.022	0.33	0.47	0.001	11	0.034	0.77
Y	0.0016	0.026	0.31	1.01	0.001	11	0.036	0.73
Er	0.0015	0.03	0.3	0.79	0.001	9	0.038	0.68
Tm	0.0015	0.04	0.29	1.18	0.01	8	0.04	0.64
Yb	0.0015	0.049	0.29	1.59	0.01	7	0.042	0.59
Lu	0.0015	0.06	0.28	1.93	0.01	6	0.044	0.51

[a]Partition coefficients from Snyder et al. (1992) and Draper et al. (2003).

from the remaining magma ocean liquid during that entire step. Thus, the end product of the crystallization stage of both major and trace element models is a set of mineral modes and averaged major and trace element compositions for the cumulates in each PCS step. The trace element composition of the last remaining liquid is also calculated assuming 98% and 99.5% crystallization of the magma ocean because this is likely to represent the evolved component present in meteorites such as Shergotty (Borg et al. 1997a, 2002, 2003).

The Trace Element Composition of Depleted Martian Mantle

Throughout this exercise, we have assumed that the martian basaltic magmas are mixtures of a component derived from a depleted mantle source composed of mafic silicates that crystallized from a magma ocean, and an evolved source represented by (crystallized) late stage liquids trapped in the cumulate pile. Thus, the first goal of the modeling is to determine if any of the cumulates have the appropriate compositions to be the depleted martian mantle (DMM) source (i.e., the source region for QUE). The trace element abundances and parent/daughter ratios calculated for the individual higher pressure cumulate packages are presented in Table 6. From Table 6, it is apparent that many of the modeled cumulates have parent/daughter ratios that are similar to those calculated for the QUE source region, although none is an exact match. Early crystallizing cumulates (PCS 1–3) have significant amounts of majoritic garnet, olivine, and orthopyroxene and, consequently, have $^{176}Lu/^{177}Hf$ ratios in excess of 0.08. This is significantly higher than the $^{176}Lu/^{177}Hf$ ratio of the QUE source region, which is estimated to be 0.048. In contrast, the last formed cumulate contains large amounts of clinopyroxene and, consequently, has a $^{176}Lu/^{177}Hf$ ratio that is ~0.028 and is, consequently, too low. The parent/daughter ratios calculated for the fourth PCS step are the best match for the QUE source region.

There are two additional criteria that can be used to determine which of the cumulates is most representative of depleted martian mantle: 1) the ability to yield melts with major element composition near Am; and 2) the presence of olivine. The presence of olivine is required because the martian basalt parental melt compositions were calculated assuming olivine saturation. Note, however, that the PCS 4 cumulates do not contain olivine. Furthermore, note that all of the cumulate packages are artificially devoid of mineralogic diversity as a result of the procedure used to define individual cumulate packages. Thus, the cumulate mineralogy and cumulate composition that are most appropriate for depleted martian mantle are a combination of cumulate packages in PCS steps 2–4. This "combined" cumulate package contains olivine, yields melts that bracket the major element parental melt composition Am, and has $^{87}Rb/^{86}Sr$, $^{147}Sm/^{144}Nd$, and $^{176}Lu/^{177}Hf$ ratios that are very similar to the QUE source region. The composition of the combined cumulate is presented in Table 6 and is hereafter referred to as depleted

Table 6. Concentrations of trace elements in cumulates and trapped liquids (ppm).[a]

Element	0–5 PCS 1	5–20 PCS 2	20–60 PCS 3	60–90 PCS 4	90–98 PCS 5	TL^{98}	$TL^{99.5}$	PCS Total	PCS 2–5	PCS 2–4 (DMM)
Rb	0.0016	0.0006	0.0011	0.044	0.46	73.2	479	0.052	0.055	0.016
Ba	0.0085	0.0030	0.0039	0.23	2.46	260	1687	0.28	0.29	0.085
Th	6E-06	7E-06	5.5E-05	0.0016	0.016	2.74	17.9	0.002	0.002	0.0006
U	2E-06	2E-06	1.6E-05	0.0009	0.0088	0.77	4.93	0.001	0.001	0.0003
Ta	0.0024	0.0009	0.0009	0.0060	0.036	1.25	7.64	0.005	0.006	0.0027
K	7.46	1.80	0.12	11.1	121	19230	125682	33.160	34.007	4.31
La	0.0042	0.0012	0.0009	0.055	0.56	17.8	107	0.063	0.066	0.020
Ce	0.025	0.0064	0.0037	0.19	1.82	48.7	289	0.210	0.220	0.069
P	201	86	56	126	550	31896	201448	130	126.031	86.2
Sr	0.016	0.0063	0.091	4.15	36.9	521	2799	4.317	4.548	1.51
Nd	0.032	0.0085	0.0062	0.24	2.11	33.6	185	0.250	0.261	0.087
Sm	0.031	0.0077	0.0030	0.12	1.00	9.88	48.5	0.123	0.128	0.046
Zr	2.31	0.62	0.15	4.47	37.3	236	994	4.689	4.817	1.76
Hf	0.076	0.020	0.0041	0.12	0.46	6.50	27.3	0.130	0.133	0.049
Eu	0.023	0.0055	0.0013	0.063	1.93	2.66	10.7	0.060	0.062	0.024
Gd	0.17	0.041	0.0062	0.28	0.33	9.57	35.8	0.261	0.266	0.11
Tb	0.024	0.0057	0.0013	0.049	0.33	1.71	6.54	0.045	0.046	0.019
Dy	0.22	0.052	0.0096	0.33	2.22	10.7	39.2	0.307	0.312	0.13
Y	2.83	0.65	0.066	1.90	12.7	65.1	248	1.886	1.836	0.82
Er	0.24	0.056	0.0082	0.21	1.35	7.22	28.0	0.198	0.195	0.086
Tm	0.058	0.013	0.0017	0.033	0.21	1.17	4.63	0.033	0.032	0.015
Yb	0.43	0.096	0.011	0.184	1.12	6.21	25.5	0.189	0.176	0.087
Lu	0.097	0.022	0.0025	0.034	0.20	1.15	4.63	0.036	0.033	0.017
$^{87}Rb/^{86}Sr$	0.293	0.298	0.035	0.031	0.036	0.408	0.497	0.035	0.035	0.031
$^{147}Sm/^{144}Nd$	0.561	0.529	0.283	0.299	0.277	0.171	0.152	0.286	0.285	0.303
$^{176}Lu/^{177}Hf$	0.1837	0.1549	0.0882	0.0404	0.0284	0.0257	0.0246	0.0403	0.0359	0.0504

[a]The QUE source is calculated to have $^{87}Rb/^{86}Sr = 0.037$, $^{147}Sm/^{144}Nd = 0.285$, and $^{176}Lu/^{177}Hf = 0.0482$.

martian mantle (DMM). Its mode is 45% orthopyroxene, 38% olivine, 14% clinopyroxene, and 3% majoritic garnet.

Figure 6b compares the incompatible-element composition of DMM to the composition of the terrestrial mid-ocean-ridge-basalt (MORB) source. The comparison is made because the MORB source is thought to represent one of the most depleted sources on Earth. Note that the overall incompatible-element pattern is very similar to the MORB source, reflecting the clinopyroxene-dominated fractionation of incompatible elements in both systems. In fact, the patterns for the depleted martian and terrestrial mantles are almost identical, with the exception of a large relative depletion of P in the MORB source. This probably reflects a difference in the abundance of P in the silicate portion of each planet.

In contrast to the incompatible-element patterns, the overall abundances of incompatible elements differ by a factor of ~10. However, this difference is consistent with the extremely low abundances of incompatible elements in many shergottites relative to MORB. This is illustrated in Fig. 6b by the overlap of average MORB composition with the composition of QUE, keeping in mind that QUE is a highly fractionated liquid with a Mg# = 38 (McSween et al. 1996), whereas average MORB is significantly less evolved. Shergottites with higher Mg#s that have not accumulated significant amounts of minerals, such as DaG 476, SaU 005, and Dhofar 019 (Dreibus et al. 2000; Zipfel et al. 2000; Taylor et al. 2002), have incompatible-element patterns that are parallel to QUE but have abundances that are ~10 times lower than either QUE or average MORB. Thus, the low incompatible-element abundances modeled for DMM are consistent with the very low abundances of these elements in the least evolved martian meteorites (i.e., those with initial Sr and Nd isotopic compositions that are similar to QUE). Unfortunately, these samples are mostly Saharan finds that have undergone significant amounts of terrestrial weathering, resulting in the addition of alkali earth elements (Dreibus et al. 2000; Zipfel et al. 2000; Crozaz and Wadhwa 2001; Wadhwa et al. 2001), and cannot be used for a detailed comparison.

The composition of liquid trapped in the cumulate pile after 98.0% and 99.5% crystallization of the magma ocean has also been calculated (Table 6). This liquid is strongly enriched in incompatible elements and, therefore, could represent the evolved component present in the martian meteorite suite. The composition of lunar KREEP (Warren and Wasson 1979) is very similar to the composition of the modeled trapped liquid after 99.5% crystallization (Fig. 6b). The KREEP composition has lower Rb, K, P, Sr, and Eu than does the modeled trapped liquid. Differences in Rb and K probably reflect the lower overall volatile-element content of the Moon compared to Mars. The lower P abundance of KREEP probably also reflects a difference in the planetary abundance of this element. Differences in Sr and Eu

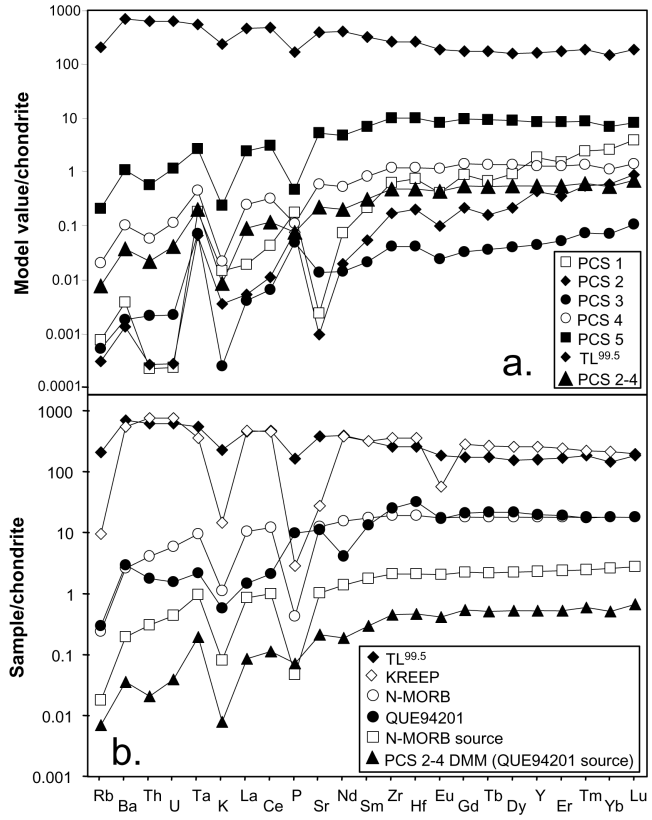

Fig. 6. a) Modeled trace element abundances of cumulate packages normalized to chondritic values of Anders and Grevesse (1989). See text for details of models; b) comparison of depleted martian mantle (DMM) composition to Earth's depleted mantle (MORB source) from Sun and McDonough (1989). Both sources have similar patterns, but QUE has elemental abundances that are ~10 times lower than MORB-source. This is consistent with incompatible-element abundances in QUE and MORB (Sun and McDonough 1989; Dreibus et al. 1996; Borg et al. 1997b), which are similar despite the fact that QUE is significantly more evolved.

abundances can be attributed to the fractionation of plagioclase from the lunar magma ocean. The fact that both Eu and Sr are depleted in lunar KREEP relative to the late stage liquid calculated for the martian magma ocean suggests that the relative Eu depletion in lunar KREEP does not simply reflect lower fO_2 in the lunar magma ocean but, rather, fractionation of a phase, such as plagioclase, in which both of these elements are relatively compatible. Despite these exceptions, the incompatible-element pattern and overall incompatible-element abundances of the modeled trapped liquid and KREEP are very similar.

Modeling Trace Element Compositions of the Martian Magmas

In this section, partial melt models are produced to investigate the composition of liquids produced by melting of the cumulates. By modeling the incompatible-element abundances of QUE, Shergotty, and ALH, the entire range of shergottite compositions will be considered. The first step in the modeling process is to strive to reproduce the incompatible-element pattern of QUE from DMM. This is because QUE has an isotopic composition that is most representative of melts derived from the most incompatible-element-depleted martian mantle. However, since this sample is highly evolved, the models do not attempt to reproduce the overall incompatible-element abundances of the QUE whole rock but, rather, abundances that are ~10 times lower. Thus, the models reproduce melts with incompatible-element abundances that are more similar to the abundances inferred for DaG 476, SaU 005, and Dhofar 019 prior to terrestrial weathering. Simple batch modal melt models are used because the uncertainties in the mode and composition of the source do not warrant the use of more sophisticated models.

The second step is to model the compositions of the martian meteorites that have incompatible-element abundances and isotopic ratios that are indicative of being derived from a more evolved source. These meteorites are inferred to contain a greater proportion of the trapped liquid component (Borg et al. 1997a, 2003). As a result, their sources are modeled as mixtures of DMM and the trapped liquid that formed after 99.5% crystallization of the magma ocean. In this case, the models attempt to reproduce the incompatible-element pattern of Shergotty and ALH. Although Shergotty is highly evolved, less evolved meteorites such as NWA 1068 have been found. This meteorite is composed of 20–30% of relatively Mg-rich olivine (Fo_{70}) but has trace element and isotopic systematics that are almost identical to Shergotty (Barrat et al. 2002; Mikouchi and Miyamoto 2002; Shih et al. 2003). The models, therefore, aim to reproduce incompatible-element abundances of Shergotty and do not attempt to account for fractionation. Likewise, since ALH is an olivine cumulate containing ~50% olivine, the models aim to reproduce incompatible-element abundances that are 2 times the bulk rock abundances.

Modeling the Trace Element Composition of the QUE 94201 Parent

Figure 7 is a plot of the incompatible-element abundances of a 10% modal partial melt of DMM. The incompatible-element abundances are normalized to DMM so that the elemental fractionation associated with melting is clearly illustrated. From Fig. 7, it is apparent that several of the incompatible-element abundances of the QUE parent are reproduced fairly well. These elements include Ba, Th, Zr, Hf, and the REEs Sm through Lu. Although not exact matches, the abundances of Sr and P are probably also within uncertainty. Several elements including Rb, U, Ta, and LREE are not reproduced by the models. Also, note that the slight depletion of MREE relative to Hf (i.e., the high Hf/Sm ratio

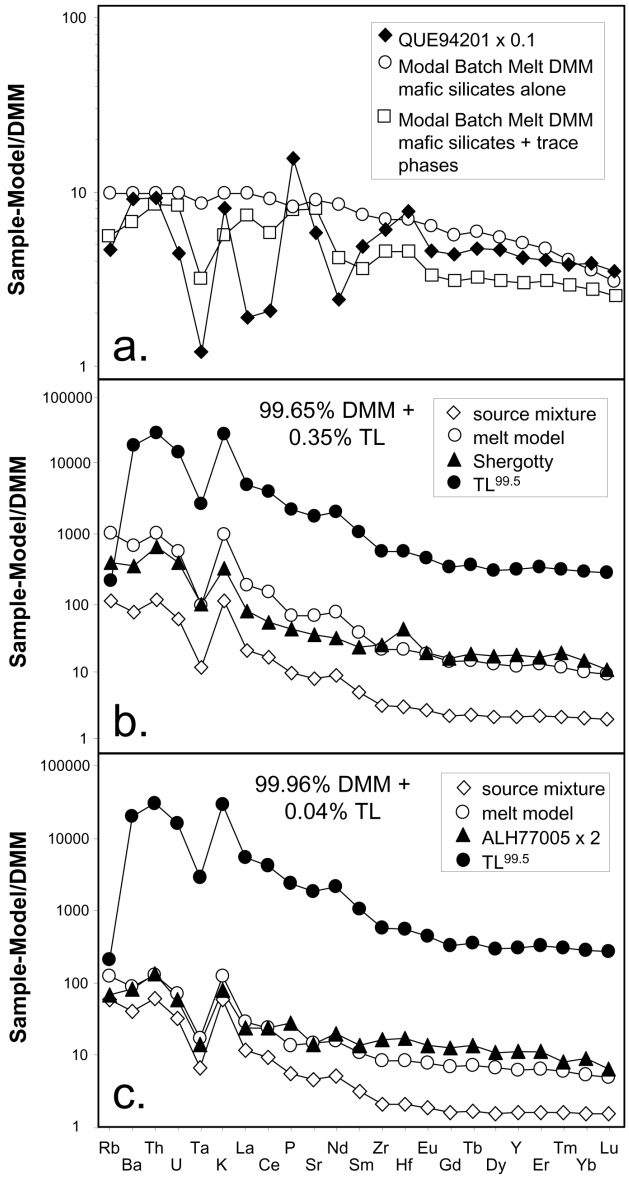

Fig. 7. Two-stage models constructed to reproduce the range of incompatible-element compositions observed in (a) QUE 94201, (b) Shergotty, and (c) ALH 77005. The abundances are normalized to DMM. The source regions of Shergotty and of ALH 77005 are modeled as mixtures of depleted martian mantle (DMM represented by the combined cumulates in PCS steps 2–4) and trapped liquid calculated after 99.5% crystallization of the magma ocean (see Fig. 6). These components are mixed together in proportions that yield a source region with $^{87}Rb/^{86}Sr$, $^{147}Sm/^{144}Nd$, and $^{176}Lu/^{177}Hf$ ratios that are closest to the meteorite being modeled. Ten percent partial melts are calculated using this source composition and the model in PCS 2–4 (orthopyroxene = 45%, olivine = 38%, clinopyroxene = 14%, and garnet/majorite = 3%). a) Model for QUE parental melt. The QUE source region has no trapped liquid and is represented by DMM. DMM has $^{87}Rb/^{86}Sr = 0.031$ (0.037), $^{147}Sm/^{144}Nd = 0.30$ (0.29), and $^{176}Lu/^{177}Hf = 0.050$ (0.048). The numbers in parentheses are parent/daughter ratios calculated for the QUE source region based on the initial Sr, Nd, and Hf isotopic compositions of the meteorite. Modeled melts are compared to the whole rock data for QUE from Borg et al. (1997a) and Dreibus et al. (1996) multiplied by a factor of 0.1 (see text). Open circles represent the composition of the modeled melt calculated assuming mineral mode of PCS 2–4 (see above). Although the model reproduces many of the elemental abundances, it does not reproduce Rb, U, or LREE abundances. Open squares represent a melt calculated assuming orthopyroxene = 45%, olivine = 30%, clinopyroxene = 14%, amphibole = 5%, garnet/majorite = 3%, phlogopite = 2%, and titanite = 1%. These phases were chosen arbitrarily because they are stabilized in terrestrial metasomatic assemblages and better reproduce the QUE whole rock incompatible-element pattern. Note that this model does not reproduce the LREE abundances. Furthermore, this model may not be realistic because trace phases are required but are unlikely to remain behind during melting; b) model for Shergotty. The Shergotty source is modeled as a mixture of 99.65% DMM and 0.35% trapped liquid and has $^{87}Rb/^{86}Sr = 0.43$ (0.37), $^{147}Sm/^{144}Nd = 0.18$ (0.18), and $^{176}Lu/^{177}Hf = 0.032$ (0.028). The data for Shergotty are from Shih et al. (1982) and Dreibus and Wänke (1982); c) model for ALH 77005. The ALH source is modeled as a mixture of 99.96% DMM and 0.04% trapped liquid and has $^{87}Rb/^{86}Sr = 0.23$ (0.22), $^{147}Sm/^{144}Nd = 0.24$ (0.22), and $^{176}Lu/^{177}Hf = 0.045$ (0.044). The data for Shergotty and ALH 77005 are from Dreibus and Wänke (1982), Smith et al. (1984), and Dreibus et al. (1992).

observed in the QUE pattern) is not reproduced by the models. Interestingly, the elements that are not reproduced well by the models are all lower than the modeled composition, consistent with either: 1) a greater compatibility of these elements in the residual assemblage; or 2) a proportional enrichment of the other elements, perhaps as a result of metasomatism. Metasomatism seems unlikely to fractionate the incompatible elements in the desired fashion, however, because the metasomatic agent is required to be enriched in high field strength elements (HFSE) and HREE (e.g., Zr, Hf, and Lu) over many large ion lithophile elements (LILE) and LREE (e.g., Rb, U, and La). This style of fractionation is uncharacteristic of terrestrial metasomatic agents, which are usually either silicate melts or hydrous fluids and are characterized by high LILE/HFSE and LREE/HREE ratios.

Alternatively, the residual mantle assemblage could contain phases in which Rb, U, Ta, and LREE are more compatible. Phases such as phlogopite, titanite, phosphate, and amphibole are commonly stabilized in the Earth's mantle during metasomatism. A melt model is constructed to investigate the potential role that these phases could play (Fig. 7). The presence of minor amounts of phlogopite and titanite in the restite yield modeled Rb, Ta, and LREE abundances in the melt that are closer to the QUE parent composition. The presence of these phases in the residual assemblage also permits the modeled DMM partial melt to generate the Hf/Sm ratio observed in QUE, as a result of the greater compatibility of Sm in an assemblage containing titanite. As the proportion of phlogopite increases, the Rb model data more closely resemble the QUE parent composition, whereas as the proportion of titanite increases, the fit of Ta and LREE improve. However, as the amount of titanite increases, the fit of K and the MREE-HREEs becomes worse. In fact, no combination of these phases ± phosphate and amphibole reproduces all of the data completely. A phase that is strongly enriched in LREE is required to reproduce the incompatible-element pattern of QUE from DMM. Thus, if a phase or phases caused the elemental fractionations observed in the QUE parent, they remain unidentified.

Modeling the Trace Element Composition of the Shergotty and ALH 77005 Parents

The incompatible-element abundances observed in Shergotty are representative of the composition of the most evolved martian basalts. As a result, the models attempt to reproduce the composition of Shergotty by melting martian mantle that is a mixture of DMM and trapped liquid. The trapped liquid composition used is that calculated after 99.5% crystallization of the magma ocean ($TL^{99.5}$). This composition was chosen because it is similar to estimates of lunar KREEP. A source with a similar composition can be obtained, however, by mixing a greater proportion of a less evolved trapped liquid (i.e., calculated after less crystallization of the magma ocean). The proportions of DMM and $TL^{99.5}$ estimated for the Shergotty source are based on the calculated parent/daughter ratios. Borg et al. (2003) estimated that Shergotty had $^{87}Rb/^{86}Sr = 0.374$, $^{147}Sm/^{144}Nd = 0.182$, and $^{176}Lu/^{177}Hf = 0.028$ (Table 1). A mixture of 99.65% DMM and 0.35% $TL^{99.5}$ has $^{87}Rb/^{86}Sr = 0.431$, $^{147}Sm/^{144}Nd = 0.177$, and $^{176}Lu/^{177}Hf = 0.032$ and is the best match to the parent/daughter ratios calculated for the Shergotty source (Table 7). This source is also assumed to have the modal mineralogy estimated for DMM.

The models demonstrate that a very small proportion of trapped liquid is required to leverage the incompatible-trace element abundances of the most evolved basaltic source region (i.e., the Shergotty source region). For example, if the Shergotty source region had 50% SiO_2 before enrichment and the trapped liquid had 100% SiO_2, then the Shergotty source region will be enriched in SiO_2 by only 0.18 wt%. Ten percent melting of the source region would result in a liquid that has a SiO_2 abundance that is only 1.8 wt% higher, assuming SiO_2 behaves incompatibly and is not involved in any incongruent melting reactions. This represents the maximum effect

Table 7. Parent/daughter ratios of modeled mixed magma ocean cumulates.[a]

Modeled and calculated meteorite sources	$^{87}Rb/^{86}Sr$	$^{147}Sm/^{144}Nd$	$^{176}Lu/^{177}Hf$
PCS 2–4 (DMM)	0.031	0.303	0.050
QUE source	0.036	0.285	0.048
99.65% DMM			
+ 0.35% TL	0.431	0.177	0.032
Shergotty source	0.374	0.182	0.028
99.96% DMM			
+ 0.04% TL	0.193	0.254	0.046
ALH 77005 source	0.183	0.217	0.044
99.97% DMM			
+ 0.003% TL	0.215	0.226	0.044
EET 79001B source	0.213	0.248	0.046

[a]Modeled trapped liquid = 99.5% PCS.

because the SiO_2 contents of the trapped liquids estimated by the major element models discussed above, as well as that estimated for lunar KREEP (Warren and Wasson 1979), are significantly less than 100 wt% (i.e., near 45–55 wt%). As a result, the major element compositions of the shergottite source regions, as well as partial melts derived from these source regions, will not be significantly affected by the addition of trapped late-stage liquid.

A 10% partial melt of this source yields a melt that is compositionally very similar to Shergotty (Fig. 7b). The modeled melt has slightly lower HREE abundances that could potentially reflect the presence of too much garnet in the model modes or a smaller majorite component in the garnet (yielding higher D_{HREE}). In addition, the abundances of the most incompatible elements, such as LILE and LREE, are slightly too high in the model composition, perhaps reflecting a slight underestimate of the melt proportions. Despite these minor differences, the model is remarkably successful in reproducing both the incompatible-element and isotopic composition of the Shergotty parental melt. The composition of ALH has also been modeled from a mixed source composed of 99.96% DMM and 0.04% $TL^{99.5}$. The parent/daughter ratios of this mixed source are very close to those calculated for the ALH source region, indicating that the modeled source will have the appropriate Sr, Nd, and Hf isotopic compositions (Table 7). The incompatible-element composition of the modeled melt is a good match for the ALH parent. Slightly lower HREE in the model may again reflect a garnet mode in the restite that is relatively high or a garnet composition that is slightly less majoritic.

The ability of these models to generate compositions that are so close to the Shergotty and ALH parental melts suggests that DMM may be a relatively accurate representation of depleted martian mantle composition. If this is correct, the inability of the models to reproduce the QUE parent from DMM seems likely to reflect problems with the cumulate melt stage of the models rather than with the cumulate crystallization stage of the models.

DISCUSSION

Comparison to Previous Model Results

Borg et al. (2003) modeled the parent/daughter ratios of the QUE source in a manner that is similar to that presented here. However, to ensure an almost perfect fit of the modeled data, they assumed that the source region contained amphibole. Amphibole was required in the source region to raise the $^{87}Rb/^{86}Sr$ ratio of the modeled QUE source region. The approach taken here is philosophically different from our previous approach. Previously, we altered the mineralogy of the cumulate package to fit the data. Here, we have estimated the mineralogy of magma ocean cumulates based on phase relationships from experiments and determined if these cumulates have trace element compositions similar to those estimated for the meteorite source regions. We emphasize that no attempt has been made to force the models to fit the data. In fact, somewhat better fits between modeled and calculated $^{87}Rb/^{86}Sr$ ratios of the meteorite sources could be obtained if small amounts of amphibole were indeed stable in the source regions. The presence of amphibole, or any Rb bearing hydrous phase, in the source regions of the meteorites is not constrained on the basis of experimental results and, therefore, violates the premise of this modeling exercise: to use experimental results to constrain the trace element and isotopic systematics of the meteorites. The models, nevertheless, are remarkably successful despite the limitations resulting from the sparse experimental constraints available.

Comparison of Lunar and Martian Differentiation

The ability of the models presented above to reproduce most of the compositional variations observed in the martian basaltic meteorite suite supports the hypothesis that initial martian planetary differentiation was associated with crystallization of a magma ocean. Similar processes have been invoked for the formation of lunar source regions, e.g., Snyder et al. (1992). Furthermore, Borg et al. (2003) demonstrated that the parent/daughter ratios calculated for the martian meteorite source regions lie along mixing curves defined by lunar mafic cumulate and lunar KREEP end members (Fig. 2). This observation indicates that despite differences in the pressure of cumulate formation and in the bulk composition of the bodies, differentiation on Mars and the Moon have yielded sources with roughly similar compositions. This is reflected in compositional similarities between martian basalts and some lunar basalts. From Fig. 8a, it is apparent that incompatible-element patterns for KREEP basalts are very similar to the patterns for Shergotty. The KREEP basalt has lower Rb, K, Sr, and Eu than Shergotty, most likely reflecting lower volatile element contents and the large scale fractionation of plagioclase on the Moon. The pattern for QUE is compared to the pattern for Apollo 15 green glass (Fig. 8b) because this liquid is thought to be derived from one of the most depleted lunar source regions. Although the MREE and HREE are a good match, the LREE and Ba, Th, and U differ significantly. This most likely reflects fractionation of these elements by an unknown process or phase on Mars.

There are also some fundamental differences between hypothetical lunar and martian magma oceans. Perhaps the most obvious is the time at which they crystallized. Martian meteorites have large isotopic anomalies in the decay products of short-lived nuclides (e.g., ^{142}Nd), indicating that silicate differentiation occurred very early. In contrast, lunar samples demonstrate less well-defined anomalies (Nyquist et al. 1993) requiring differentiation to have occurred later, or to have been less efficient, on the Moon than on Mars. This most likely reflects the formation of the Moon after the formation of Mars

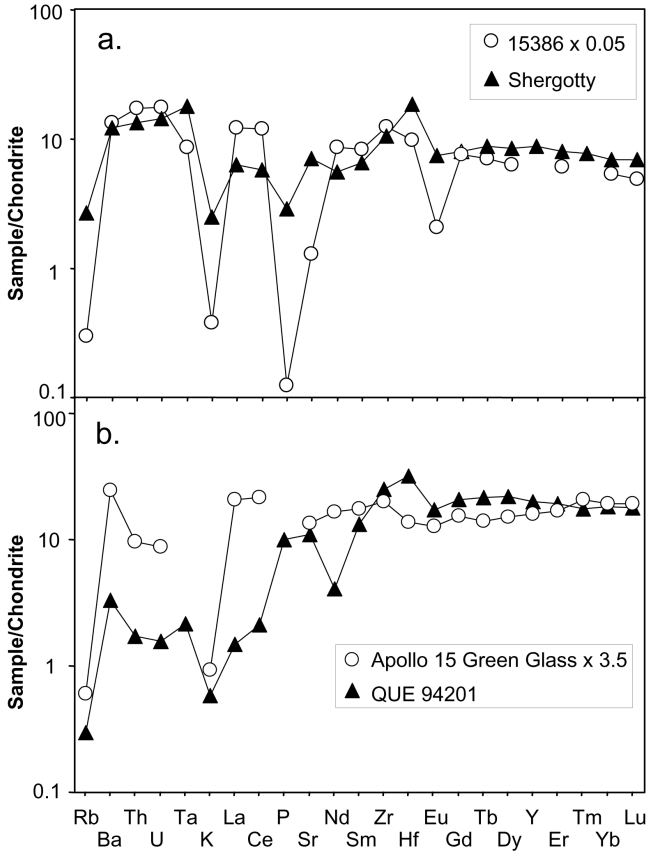

Fig. 8. A comparison of lunar and martian basalt incompatible-element patterns: a) whole rock incompatible-element abundances of Shergotty and Apollo 15 KREEP basalt 15386 from Warren and Wasson (1978). The elemental abundances of 15386 are multiplied by 0.05 to permit a better comparison of the patterns. Higher overall incompatible-element abundances in 15386 most likely reflect a greater proportion of trapped liquid (KREEP) in this magma. Note the close similarity between the patterns. Elements that have lower abundances in 15386 than in Shergotty are Rb, K, P, Sr, and Eu. The deviations are most likely due to differences in the elemental abundances in the silicate portion of Mars and the Moon or to the large scale fractionation of plagioclase on the lunar magma ocean; b) whole rock incompatible-element abundances of QUE 94201 and Apollo 15 green glass from Ma et al. (1981). The green glass abundances have been multiplied by 3.5 for comparison and to account for fractionation of QUE. A good general agreement exists between 2 patterns with the exception of Ba, Th, U, La, Ce, and Nd, which are lower in QUE. This could reflect the higher compatibility of these elements in the martian mantle due to the presence of an unknown phase.

as predicted by the giant impact hypothesis (Snyder et al. 2000). Another significant difference is the relatively major role that plagioclase plays in lunar differentiation. As discussed above, the higher pressure crystallization regime expected for a martian magma ocean, combined with early depletion of Al_2O_3 in the magma ocean by garnet crystallization, may inhibit large amounts of plagioclase crystallization. Plagioclase stability could be further limited on Mars by the relatively volatile-rich (and presumably water-rich) nature of the bulk planet. Thus, that small dry bodies like the Moon show abundant evidence for plagioclase crystallization is not unexpected, whereas larger planets, like Mars, seem to lack evidence for plagioclase crystallization.

Another seemingly unique characteristic of some lunar sources is their ilmenite-rich modes that result in magmas with very high Fe and Ti abundances. Although ilmenite is likely to crystallize during the late stages of a martian magma ocean, martian samples derived from such sources have not been found. This could simply reflect a sampling bias. Alternatively, it could reflect the presence of less ilmenite in the martian magma ocean. The relatively high ilmenite mode of the lunar magma ocean reflects the domination of the late crystallization stages by plagioclase, a phase that does not contain significant amounts of either Fe or Ti and, therefore, produces late stage liquids that are strongly enriched in these elements. In contrast, the late stages of martian magma ocean crystallization are dominated by clinopyroxene in which both Fe and Ti are compatible.

Ramifications of a Martian Magma Ocean

The presence of a martian magma ocean is appealing because it permits extensive fractionation of elements to occur very early in the history of the planet. It also provides an explanation for why individual crystallization products have remained isolated until the time of magma formation; they simply have not been melted since formation (Borg et al. 1997a). However, defining a mechanism by which a large portion of Mars is heated above its liquidus temperature is problematic. In the case of the Moon, significant heat can be added to the system by a giant impact. The preservation of isotopic anomalies from short-lived isotopic systems in the martian meteorites precludes invoking a giant impact as the heat source for Mars because such an impact would erase these anomalies.

Two common heat sources that have been considered in thermal modeling of Mars are heat from accretion and heat from the decay of short-lived nuclides such as ^{26}Al and ^{60}Fe. The amount of heat available from these sources is indirectly proportional to the time scale of accretion. Although very rapid accretion contrasts with some models of planetary accretion (e.g., Wetherill 1980), it is consistent with the concept of runaway accretion that allows bodies to attain large sizes in relatively short periods of time (e.g., Wetherill 1988). In fact, Ghosh et al. (2003) suggested that Mars could have accreted 3 Ma after CAI formation, a timescale that may be required to account for a deep martian magma ocean.

CONCLUSION

The major element, trace element, and isotopic systematics of the basaltic martian meteorites are consistent with derivation by melting of mixtures of cumulates and late stage liquids that crystallized at ~4.5 Ga from a magma ocean.

In order to obtain parental melts with superchrondritic CaO/Al_2O_3 ratios and high Mg#s, garnet must be a liquidus or near-liquidus phase during magma-ocean crystallization. This suggests that the pressure at the base of the magma ocean was at least 12 GPa. Cumulates crystallizing after an initial stage of garnet crystallization and containing olivine, orthopyroxene, clinopyroxene, and minor amounts of garnet have parent/daughter ratios that are similar to those calculated for the most depleted martian source region. The mineral modes and major and trace element compositions calculated for this source region are a reasonable approximation for depleted martian mantle (DMM) composition. Terrestrial depleted mantle source regions have similar incompatible-element ratios but have higher overall incompatible-element abundances. This is consistent with the lower abundances of these elements in martian parental melts compared to parental melts of terrestrial depleted source regions. The compositional range observed in the incompatible element and isotopic systematics of the martian meteorites reflects the progressive incorporation of trapped liquid into their source regions. The limited amount of late-stage liquid that is required to produce the parent/daughter ratios calculated for the martian basalt sources precludes the major-element compositions of the source regions from being altered dramatically. Although the martian magma ocean is, in many ways, similar to the lunar magma ocean, fundamental mineralogical and compositional differences exist as a result of a higher pressure of crystallization and a higher volatile element content for Mars.

Acknowledgments–We wish to thank H. Y. McSween, Jr. for his constructive review. We are also grateful for J. J. Papike's informal review and for helpful discussions with him and with C. K. Shearer and C. B. Agee. We also appreciate the efforts of A. Treiman and C. Herd in organizing the "Unmixing the SNCs" workshop. Support for this project was provided by the NASA Cosmochemistry Program (grant NAG5–11155).

Editorial Handling—Dr. Urs Krähenbühl

REFERENCES

Agee C. B. and Draper D. S. Forthcoming. Partial melting of Homestead L5 ordinary chondrite: Implications for mantle differentiation on Mars. *Earth and Planetary Science Letters.*

Agee C. B., Li J., Shannon M. C., and Circone S. 1995. Pressure-temperature phase diagram for the Allende meteorite. *Journal of Geophysical Research* 100:17725–17740.

Anders E. and Grevesse N. 1989. Abundances of the elements: Meteoritic and solar. *Geochimica et Cosmochimica Acta* 53:197–214.

Barrat J. A., Jambon A., Bohn M., Gillet P., Sautter V., Goepel C., Lesourd M., and Keller F. 2002. Petrology and chemistry of the picritic shergottite Northwest Africa 1068 (NWA 1068). *Geochimica et Cosmochimica Acta* 66:3505–3518.

Bertka C. M. and Fei Y. 1997. Mineralogy of the martian interior up to core-mantle boundary pressures. *Journal of Geophysical Research* 102:5251–5264.

Bertka C. M. and Holloway J. R. 1994a. Anhydrous partial melting of an iron-rich mantle; I, Subsolidus phase assemblages and partial melting phase relations at 10 at 30 kbar. *Contributions to Mineralogy and Petrology* 115:313–322.

Bertka C. M. and Holloway J. R. 1994b. Anhydrous partial melting of an iron-rich mantle; II, Primary melt compositions at 15 kbar. *Contributions to Mineralogy and Petrology* 115:323–338.

Blichert-Toft J., Gleason J. D., Telouk P., and Albarede F. 1999. The Lu-Hf isotope geochemistry of shergottites and the evolution of the martian mantle-crust system. *Earth and Planetary Science Letters* 173:25–39.

Borg L. E., Nyquist L. E., Taylor L. A., Wiesmann H., and Shih C. Y. 1997a. Constraints on martian differentiation processes from Rb-Sr and Sm-Nd isotopic analyses of the basaltic shergottite QUE 94201. *Geochimica et Cosmochimica Acta* 61:4915–4931.

Borg L. E., Nyquist L. E., Taylor L. A., Wiesmann H., and Shih C. Y. 1997b. Rb-Sr and Sm-Nd isotopic analyses of QUE 94201; Constraints on martian differentiation processes. 28th Lunar and Planetary Science Conference. pp. 133–134.

Borg L. E., Nyquist L. E., Wiesmann H., and Reese Y. 2002. Constraints on the petrogenesis of martian meteorites from the Rb-Sr and Sm-Nd isotopic systematics of the lherzolitic shergottites ALH 77005 and LEW 88516. *Geochimica et Cosmochimica Act*a 66:2037–2053.

Borg L. E., Nyquist L. E., Reese Y., and Wiesmann H. 2003. The age of Dar al Gani 476 and the differentiation history of the martian meteorites inferred from their Rb-Sr, Sm-Nd, and Lu-Hf isotopic systematics. *Geochimica et Cosmochimica Acta* 67: 3519–3536.

Brandon A. D., Walker R. J., Morgan J. W., and Goles G. G. 2000. Re-Os isotopic evidence for early differentiation of the martian mantle. *Geochimica et Cosmochimica Acta* 64:4083–4095.

Crozaz G. and Wadhwa M. 2001. The terrestrial alteration of Saharan shergottites Dar al Gani 476 and 489; A case study of weathering in a hot desert environment. *Geochimica et Cosmochimica Acta* 65:971–977.

Draper D. S., Chabot N. L., Xirouchakis D., Wasserman A. A., and Agee C. B. 2001. Partitioning of Nd, Tb, Lu, and Hf between garnet and ordinary chondrite melt at 5 to 9 GPa: Applications to martian differentiation (abstract #1681). 32nd Lunar and Planetary Science Conference.

Draper D. S. and Johnston A. D. 1992. Anhydrous PT phase relations of an Aleutian high-MgO basalt; An investigation of the role of olivine-liquid reaction in the generation of arc high-alumina basalts. *Contributions to Mineralogy and Petrology* 112:501–519.

Draper D. S., Xirouchakis D., and Agee C. B. 2003. Trace element partitioning between garnet and chondritic melt from 5 to 9 GPa: Implications for the onset of the majorite transition in the martian mantle. *Physics of the Earth and Planetary Interiors* 139:149–169.

Dreibus G., Jagoutz E., Spettel B., and Waenke H. 1996. Phosphate-mobilization on Mars? Implication from leach experiments on SNCs. 27th Lunar and Planetary Science Conference. pp. 323–324.

Dreibus G., Jochum K. H., Palme H., Spettel B., Wlotzka F., and Waenke H. 1992. LEW 88516; A meteorite compositionally close to the "martian mantle." *Meteoritics* 27:216–217.

Dreibus G., Spettel B., Haubold R., Jochum K. P., Palme H., Wolf D. and Zipfel J. 2000. Chemistry of a new shergottite; Sayh al Uhaymir 005 (abstract #5024). 63rd Annual Meteoritical Society Meeting.

Dreibus G. and Wänke H. 1982. Parent body of the SNC-meteorites;

Chemistry, size and formation. 45th Annual Meteoritical Society Meeting. pp. 207–208.
Dreibus G. and Wänke H. 1985. Mars, a volatile-rich planet. *Hans Suess Festschrift* 20:367–381.
Ghosh A., Nimmo F., and McSween H. Y. J. 2003. The effect of early accretion and redistribution of ^{26}Al on the thermal evolution of Mars (abstract #2011). 33rd Lunar and Planetary Science conference. CD-ROM.
Gilpin L., Bertka C. M., Minitti M., and Fei Y. 2001. Melting of a model orthopyroxene-rich martian mantle at 2.0 GPa (abstract #1717). 32nd Lunar and Planetary Science Conference. CD-ROM.
Green T. H. and Pearson N. J. 1987. An experimental study of Nb and Ta partitioning between Ti-rich minerals and silicate liquids at high pressure and temperature. *Geochimica et Cosmochimica Acta* 51:55–62.
Harper C. L., Jr., Nyquist L. E., Bansal B., Wiesmann H. and Shih C. Y. 1995. Rapid accretion and early differentiation of Mars indicated by ^{142}Nd/^{144}Nd in SNC meteorites. *Science* 267:213–217.
Harvey R. P., Wadhwa M., McSween H. Y., Jr., and Crozaz G. 1993. Petrography, mineral chemistry, and petrogenesis of Antarctic shergottite LEW 88516. *Geochimica et Cosmochimica Acta* 57: 4769–4783.
Herd C. D. K., Borg L. E., Jones J. H., and Papike J. J. 2002. Oxygen fugacity and geochemical variations in the martian basalts: Implications for martian basalt petrogenesis and the oxidation state of the upper mantle of Mars. *Geochimica et Cosmochimica Acta* 66:2025–2036.
Herzberg C. and Zhang J. 1996. Melting experiments on anhydrous peridotite KLB-1; Composition of magmas in the upper mantle and transition zone. *Journal of Geophysical Research* 101:8271–8295.
Hess P. 2002. Origins of the martian crust and mantle (abstract #6029). Workshop on Unmixing the SNCs: Chemical, Isotopic, and Petrologic Components of the Martian Meteorites. Lunar and Planetary Institute Contribution #1134. pp. 23–24.
Jarosewich E. and Dodd R. T. 1981. Chemical variations among L-group chondrites; II, Chemical distinctions between L3 and LL3 chondrites. *Meteoritics* 16:83–91.
Jarosewich E. and Dodd R. T. 1985. Chemical variations among L chondrites; IV, Analyses, with petrographic notes, of 13 L-group and 3 LL-group chondrites. *Meteoritics* 20:23–36.
Johnson M. C., Rutherford M. J., and Hess P. C. 1991. Chassigny petrogenesis; Melt compositions, intensive parameters, and water contents of martian (?) magmas. *Geochimica et Cosmochimica Acta* 55:349–366.
Jones J. H. 1989. Isotopic relationships among the shergottites, the nakhlites, and chassigny. 19th Lunar and Planetary Science Conference. pp. 465–474.
Lodders K. and Fegley B. 1997. An oxygen isotope model for the composition of Mars. *Icarus* 126:373–394.
Lodders K. and Fegley B. 1998. *The planetary scientist's companion.* New York: Oxford University Press. 371 p.
Longhi J., Knittle E., Holloway J. R., Waenke H., and Gehrels T. 1992. The bulk composition, mineralogy, and internal structure of Mars. In *Mars,* edited by Kieffer H. H., Jakowsky B. M., Snyder C., and Matthews M. S. Tucson: University of Arizona Press. pp. 184–208.
Longhi J. and Pan V. 1988. The parental magmas of the SNC Meteorites. 19th Lunar and Planetary Science Conference. pp. 690–691.
Longhi J. and Pan V. 1989. The parent magmas of the SNC meteorites. 19th Lunar and Planetary Science Conference. pp. 451–464.
Ma M. S., Liu Y. G., and Schmitt R. A. 1981. A chemical study of individual green glasses and brown glasses from 15426; Implications for their petrogenesis. 12th Lunar and Planetary Science Conference. pp. 915–933.
McSween H. Y., Jr. 1985. SNC meteorites: Clues to martian petrologic evolution? *Reviews of Geophysics* 23:391–416.
McSween H. Y., Jr. 1994. What we have learned about Mars from SNC meteorites. *Meteoritics* 29:757–779.
McSween H. Y., Jr. and Jarosewich E. 1983. Petrogenesis of the Elephant Moraine A79001 meteorite: multiple magma pulses on the shergottite parent body. *Geochimica et Cosmochimica Acta* 47:1501–1513.
McSween H. Y., Jr., Lundberg L. L., and Crozaz G. 1988. Crystallization of the ALH A77005 shergottite: How closed is a closed system? 19th Lunar and Planetary Science Conference. pp. 766–767.
McSween H. Y., Jr., Eisenhour D. D., Taylor L. A., Wadhwa M., and Crozaz G. 1996. QUE 94201 shergottite; Crystallization of a martian basaltic magma. *Geochimica et Cosmochimica Acta* 60: 4563–4569.
McSween H. Y. J., Grove T. L., and Wyatt M. B. 2003. Constraints on the composition and petrogenesis of the martian crust. *Journal of Geophysical Research* 108:9-1–9-19.
Meyer C. 2003. *Mars meteorite compendium.* Houston: NASA Johnson Space Center. Report 27672 (rev. B).
Mikouchi T. and Miyamoto M. 2002. Olivine cooling rate of the Northwest Africa 1068 shergottite (abstract #1562). 33rd Lunar and Planetary Science Conference. CD-ROM.
Nyquist L. E., Bansal B. M., Wiesmann H., and Shih C. Y. 1995. "Martians" young and old; Zagami and ALH 84001. 26th Lunar and Planetary Science Conference. pp. 1065–1066.
Nyquist L. E., Bogard D. D., Wooden J. L., Wiesmann H., Shih C. Y., Bansal B. M., and McKay G. 1979. Early differentiation, late magmatism, and recent bombardment on the shergottite parent planet. 42nd Annual Meteoritical Society Meeting. pp. 502.
Nyquist L. E., Reese Y., Wiesmann H., and Shih C. Y. 2001. Age of EET 79001B and implications for shergottite origins (abstract #1407). 32nd Lunar and Planetary Science Conference. CD-ROM.
Nyquist L. E., Reese Y. D., Wiesmann H., Shih C. Y., and Schwandt C. 2000. Rubidium-strontium age of the Los Angeles shergottite. 63rd Annual Meteoritical Society Meeting. pp. 121–122.
Nyquist L. E., Shih C. Y., Wiesmann H., and Bansal B. M. 1993. ^{146,147}Sm-^{142,143}Nd formation interval for the lunar mantle and implications for lunar evolution. 24th Lunar and Planetary Science Conference. pp. 1095–1096.
Ohtani E., Kawabe I., Moriyama J., and Nagata Y. 1989. Partitioning of elements between majorite garnet and melt and implications for petrogenesis of komatiite. *Contributions to Mineralogy and Petrology* 103:263–269.
Ohtani E., Nagata Y., Suzuki A., and Kato T. 1995. Melting relations of peridotite and the density crossover in planetary mantles. *Chemical Geology* 120:207–221.
Schwandt C. S., Jones J. H., Mittlefehldt D. W., and Treiman A. H. 2001. The magma composition of EET 79001A; The first recount (abstract #1913). 32nd Lunar and Planetary Science Conference. CD-ROM.
Shih C. Y., Nyquist L. E., Bogard D. D., McKay G. A., Wooden J. L., Bansal B. M., and Wiesmann H. 1982. Chronology and petrogenesis of young achondrites, Shergotty, Zagami, and ALH A77005; Late magmatism on a geologically active planet. *Geochimica et Cosmochimica Acta* 46:2323–2344.
Shih C. Y., Nyquist L. E., Wiesmann H., and Barrat J. A. 2003. Age and petrogenesis of picritic shergottite NWA 1068: Sm-Nd and

Rb-Sr isotopic studies (abstract #1439). 34th Lunar and Planetary Science Conference. CD-ROM.

Smith M. R., Laul J. C., Ma M. S., Huston T., Verkouteren R. M., Lipschutz M. E., and Schmitt R. A. 1984. Petrogenesis of the SNC (shergottites, nakhlites, chassignites) meteorites; Implications for their origin from a large dynamic planet, possibly Mars. 14th Lunar and Planetary Science Conference,. pp. 612–630.

Snyder G. A., Borg L. E., Nyquist L. E., and Taylor L. A. 2000. Chronologic and isotopic constraints on lunar evolution. In *Origin of the Earth and Moon,* edited by Canup R. M. and Righter K.. Tuscon: University of Arizona Press. pp. 361–396.

Snyder G. A., Taylor L. A., and Neal C. R. 1992. A chemical model for generating the sources of mare basalts: Combined equilibrium and fractional crystallization of the lunar magmasphere. *Geochimica et Cosmochimica Acta* 56:3809–3823.

Stolper E. and McSween H. Y., Jr. 1979. Petrology and origin of the shergottite meteorites. *Geochimica et Cosmochimica Acta* 43: 1475–1498.

Sun S. S. and McDonough W. F. 1989. Chemical and isotopic systematics of oceanic basalts; Implications for mantle composition and processes. In *Magmatism in the ocean basins.* London: Geological Society of London. Special Publication 42. pp. 313–345.

Taylor L. A., Nazarov M. A., Shearer C. K., McSween H. Y., Jr., Cahill J., Neal C. R., Ivanova M. A., Barsukova L. D., Lentz R. C., Clayton R. N., and Mayeda T. K. 2002. Martian meteorite Dhofar 019; A new shergottite. *Meteoritics & Planetary Science* 37:1107–1128.

Treiman A. H. 1986. The parental magma of the Nakhla achondrite: Ultrabasic volcanism on the shergottite parent body. *Geochimica et Cosmochimica Acta* 50:1061–1070.

Wadhwa M., Lentz R. C. F., McSween H. Y., Jr., and Crozaz G. 2001. A petrologic and trace element study of Dar al Gani 476 and Dar al Gani 489; Twin meteorites with affinities to basaltic and lherzolitic shergottites. *Meteoritics & Planetary Science* 36:195–208.

Warren P. H. and Wasson J. T. 1978. Compositional-petrographic investigation of pristine nonmare rocks. 9th Lunar and Planetary Science Conference. pp. 185–217.

Warren P. H. and Wasson J. T. 1979. The origin of KREEP. *Reviews of Geophysics and Space Physics* 17:73–88.

Wasserman A. A., Chabot N. L., Draper D. S., and Agee C. B. 2001. High pressure anhydrous phase relations of homestead L5: An analogue for martian mantle (abstract #2029). 32nd Lunar and Planetary Science Conference. CD-ROM.

Wetherill G. W. 1980. Numerical calculations relevant to the accumulation of the terrestrial planets. In *The continental crust and its mineral deposits,* edited by D. W. Strangway. Newfoundland: Geological Association of Canada. pp. 3–24.

Wetherill G. W. 1988. Accumulation of Mercury from planetesimals. In *Mercury,* edited by Vilas F., Chapman C. R., and Matthews M. S. Tucson: University of Arizona Press. pp. 670–691.

Wooden J. L., Ashwal L. D., Wiesmann H., and Shih C. Y. 1982. Metamorphic disturbance of Rb-Sr and Sm-Nd isotopic systematics. In *Geological Association of Canada; Mineralogical Association of Canada; Joint Annual Meeting,* edited by Brisbin W. C. Newfoundland: Geological Association of Canada. pp. 87.

Zhang J. and Herzberg C. 1994. Melting experiments on anhydrous peridotite KLB-1 from 5.0 to 22.5 GPa. *Journal of Geophysical Research* 99:17729–17742.

Zipfel J., Scherer P., Spettel B., Dreibus G., and Schultz L. 2000. Petrology and chemistry of the new shergottite Dar al Gani 476. *Meteoritics & Planetary Science* 35:95–106.